



Pseudoline parameters to represent n-butane (n-C₄H₁₀) cross-sections measured in the 7–15 μm region for the Titan atmosphere

Keeyoon Sung^{a,*}, Brendan Steffens^b, Geoffrey C. Toon^a, Deacon J. Nemchick^a, Mary Ann H. Smith^c

^aJet Propulsion Laboratory, California Institute of Technology, Pasadena, CA, USA

^bFlorida Institute of Technology, 150 W University Blvd, Melbourne, FL, USA

^cScience Directorate, NASA Langley Research Center, Hampton, VA, USA

ARTICLE INFO

Article history:

Received 20 February 2020

Revised 2 April 2020

Accepted 2 April 2020

Available online 16 May 2020

Keywords:

n-Butane
FT-IR spectrum
Cross section
Pseudolines
Bruker I25HR
Cassini/CIRS
Titan
Hydrocarbons

ABSTRACT

We measured temperature-dependent cross-sections of n-butane (CH₃–CH₂–CH₂–CH₃) in the mid-infrared (7–15 μm) region in support of remote sensing for the Titan's atmosphere. For this, 28 pure and N₂-mixture spectra were obtained at 180–298 K using a high-resolution Fourier transform spectrometer (Bruker IFS 125 HR) at the Jet Propulsion Laboratory. The spectral resolutions were selected to be between 0.0039 and 0.06 cm⁻¹, depending on the sample pressures. The observed spectra were fit simultaneously to generate one single set of pseudolines, which include line intensities and lower state energies at individual pseudoline positions. The observed spectra could be reproduced by the pseudolines to within 4% through line-by-line radiative transfer calculations. The integrated intensities at 296 K were measured to be 5.06(28), 7.18(27), 0.91(4), and 49.01(20) × 10⁻¹⁹ cm⁻¹/(molecule.cm⁻²) in the 660–860, 860–1060, 1060–1200, and 1200–1538 cm⁻¹ regions, respectively, by summing up the pseudoline intensity parameters. These results are observed to be significantly lower than that of the PNNL (Pacific Northwest National Laboratory) cross-sections obtained at low resolution. The pseudolines are electronically compiled in the HITRAN database format, which can be readily integrated with existing radiative transfer calculations. The measured cross-sections represented by the pseudolines could provide critical laboratory input in search of elusive species that might be captured in the Cassini/CIRS and the JWST/MIRI spectral observations.

© 2020 Elsevier Ltd. All rights reserved.

1. Introduction

The atmosphere of Titan, with its rich organic chemistry initiated through photolysis and photosensitized dissociation of CH₄, is of great interest to planetary science. A number of atmospheric properties of Titan, whose dominant constituent is N₂ like as in the Earth atmosphere, suggest that it may resemble the prebiotic Earth [1]. Thus, understanding the Titan atmosphere through observations, modeling, and laboratory spectroscopic work would provide a useful insight into the early Earth environment and even the origin of life.

Photochemistry in Titan's stratosphere is driven by solar UV radiation, which leads to ionization of N₂ and CH₄ followed by various chain reactions during the downward flow of the intermediate

products. Hydrocarbons, which originate primarily from photodissociation of the methane in the upper atmosphere, are an important element of Titan's stratosphere [2]. The distributions of these hydrocarbons have been investigated thoroughly through modeling work for decades [3–11]. The seminal photochemical modeling paper on Titan's atmosphere by Yung and Allen [4] draws specific attention to the high abundance predicted for butane, arising from the same chemistry that produces the propane, which has already been observed [12,13]. Later models [5,11,14], predict that butane is generated at a comparable production rate to that of propane in the atmosphere of Titan. We note that the disk averaged abundance of propane was observed to be 476 ppb by Cassini/CIRS, about ~100 times higher than the Cassini/CIRS detection sensitivity [15]. Since the production rate of butane was estimated to be only seven time lower than that of the abundant propane in Titan's atmosphere [5], the detection of butane is anticipated from the Cassini/CIRS and JWST/MIRI observations [16]. Now, butane is investigated in more sophisticated photochemistry models for Titan atmosphere as one of key hydrocarbons [9,11,17].

* Corresponding author at: M/S 200-105, 4800 Oak Grove Dr. Jet Propulsion Laboratory, California Institute of Technology, USA.

E-mail address: ksung@jpl.nasa.gov (K. Sung).

Specific chemical mechanisms for the production of butane in the atmosphere of Titan have been proposed as well, for instance, through the addition of methyl and propyl radicals [11]. Butane has also been shown to form naturally when a methane sample is irradiated by UV light in experimental conditions similar to that of the Titan atmosphere [18,19]. In the laboratory experiment by Adamkovic et al. [18], the net production rate of butane was observed to be 1.3×10^{10} cm³/sec, almost 50 times greater than that of propyne (C₃H₄), which was already detected in abundance by Voyager/IRIS. In fact, butane is predicted to be the most abundant C₄-hydrocarbon in the photochemistry modeling of Saturn as well [20]. Additionally, it has been shown that butane's high freezing point can even play a role in nucleation into haze particles in Titan's atmosphere [21]. Along with acetylene, butane has been proposed to be a good candidate for species that could compose the surface of the evaporite of Titan [22]. With abundances of propane and butane being predicted by multiple models, and with multiple production channels identified and even simulated in the lab, explicit detection of butane at Titan is highly anticipated for the near future.

Such detection of butane would likely come from the Cassini/CIRS observations and JWST/MIRI to come [16], the former of which has helped to constrain atmospheric models for Titan. For these observations to be properly interpreted, however, the spectra of both butane isomers (n-butane and isobutane) must be rigorously studied. The 2500–3280 cm⁻¹ region for isobutane has been explored recently at temperatures (200–300 K) and pressures (~10 Torr) appropriate for Titan [23,24]. Little work has been done, however, in the 7–15 μm region of n-butane at cold temperatures. Applying quantum-mechanical modeling via empirical Hamiltonians [25,26] to produce precision spectroscopy is challenging for polyatomic hydrocarbons such as n-butane. The n-butane has two conformers (*trans* and *gauche*) and each has three low-lying torsional states, which generate numerous hot and combination bands even in the mid-infrared region, making their spectroscopic features intractable. For these hydrocarbons, however, their contributions from the hot-band and combination band features cannot be neglected even at cold temperatures because of the generic low-lying states involving the torsional states. In order to capture the spectroscopic features as a whole, we have instead measured absorption cross-sections for n-butane at cold temperatures down to 180 K. The experimental details are presented in Section 2, while the derivation of cross-sections from these data is discussed in Section 3. We have taken an additional step to make our results more useful for line-by-line calculations by generating pseudolines in the format adopted in the HITRAN spectroscopic line parameter database [27]. Until true spectroscopic line parameters are available, these pseudolines can serve as a practical and effective alternative in radiative transfer calculations [28–32]. The pseudoline list is described in Section 4, along with the integrated cross-sections and comparison with those of the PNNL database [33] presented in Section 5.

2. Experimental details

We obtained 28 high-resolution spectra of pure n-butane (n-C₄H₁₀) sample and its mixtures with N₂ at temperatures between 298 K and 180 K in increments of ~25 K using a Fourier-transform infrared spectrometer (FT-IR), Bruker IFS-125HR, at the Jet Propulsion Laboratory (JPL). The high purity sample of n-butane (n-C₄H₁₀, CAS-No.: 106-97-8) in a stated purity of 99% was purchased from Sigma Aldrich, Inc., which came with no additional document on possible impurities of CO₂ or other hydrocarbons. During the data acquisition, however, we noticed distinctive features from CO₂ in the ν₂ band near 667 cm⁻¹, whose impurity was later estimated to be 0.03% of the sample pressure. The CO₂ features showed up

Table 1

Instrumental configuration of the Bruker 125 HR and the cold cell.

Spectral region	650–1550 cm ⁻¹
# of spectra	28 (11 pure and 17 N ₂ -mixture)
IR source	Globar
Beam Splitter	KBr
Resolution	0.0039, 0.008, 0.06 cm ⁻¹
Aperture (dia.)	2.5–2.0 mm
Cell length	20.38 cm
Windows (wedged)	ZnSe for the cell; KBr for the vacuum box
Detectors	HgCdTe (LN ₂ cooled)
Sample and purity	n-C ₄ H ₁₀ (99%), N ₂ (99.9999%)
FTS pressure	< 10 mTorr (including residual H ₂ O)

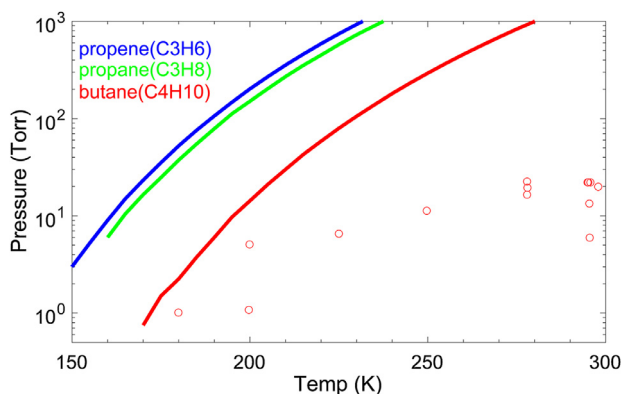
very well localized, being apart from one of the n-butane bands at 732 cm⁻¹, and they were effectively fitted out during the analysis of the spectrum set in generating pseudoline lists as will be discussed in Section 4. Out of the 28 spectra, 17 n-butane spectra were broadened with research-grade (99.99995%) N₂ sample gas.

For an absorption gas cell, the same 20.38 cm path long cryogenic copper cell was used in this work as in our earlier work on propane (C₃H₈) and propene (C₃H₆) [30,32], whose detailed characterization and performance properties can be found elsewhere [30,33]. Only a brief description is placed here: the cell has a pair of wedged ZnSe windows and is housed in a separate vacuum box with KBr windows to protect the cold windows from collecting cryodeposits while being cold. The cell temperature was regulated by a closed-cycle helium-cooled refrigerator and a heater attached to the cell body. Two silicon-diode temperature sensors were attached to the cell body; one close to a heat reservoir connected to the cold finger of the cell for temperature control feedback loop, the other to the cell body farthest away from the heater as a gas sample temperature indicator. It showed excellent temperature regulation, e.g., temperature stability better than 0.1 K for several days. As summarized in Table 1, the interferometer, Bruker 125HR, was configured with a Globar infrared source, a KBr beam splitter, and a liquid N₂-cooled detector, MCT (Mercury Cadmium Telluride). The maximum optical path differences (MOPD) of 128.6, 64.3, and 8.04 cm were used, which provided unapodized spectral resolutions of 0.0039, 0.008, 0.06 cm⁻¹, respectively. An optical filter encompassing the 650–1550 cm⁻¹ region was used to obtain the desired bandpass. The aperture diameter was set to be 2.5 mm for all spectra. The entirety of the optical beam path running through the Bruker FT-IR chambers was evacuated to a pressure of approximately 10 mTorr during the experiment, which effectively, but not completely, suppressed strong water transitions in the ν₂ band arisen from the residual water vapor in the Bruker FTS chambers.

Sample pressures were continually monitored using three sets of MKS Baratron transducers with 0–10, 0–100 and 0–1000 Torr pressure ranges. Various total pressures and volume mixing ratios were prescribed to obtain sufficient optical density at the desired experimental conditions, summarized in Table 2. Pure sample spectra (with no discrimination of *trans* and *gauche* conformers) were first measured at a given temperature, and then measured again after adding N₂ to get the desired mixture pressures. Insertion of the n-butane and N₂ gas samples was executed by following a standard operating procedure developed in an effort to minimize uncertainties in the n-butane partial pressures for the individual mixtures. For example, a sample inlet tube was evacuated up to a shut-off valve for the cell every time after each pure n-butane insertion. When preparing admixtures, the sample line was pressurized with N₂ to the shut-off valve to prevent any possible re-flux of the existing sample of the cell. Finally, the partial pressure of n-butane for each mixture spectrum was obtained from the initial value of the pure n-butane sample for the ensuing mixture spec-

Table 2Experimental conditions of the pure and N₂-broadened n-C₄H₁₀ spectra (with no discrimination of *trans* and *gauche* conformers).

Spectra	650–1550 cm ⁻¹			Resolution (cm ⁻¹)
	T (K)	P _s (Torr)	P _t (Torr)	
Pure sample spectra				
B0174.1a	295.5(3)	13.26(5)		0.0039
B0174.1b	295.2(3)	21.90(2)		0.0039
B0174.6a	298.0(3)	19.75(3)		0.062
B0174.2a	278.0(1)	16.35(3)		0.0039
B0174.2d	278.0(1)	22.35(9)		0.0039
B0174.7a	278.1(1)	19.27(1)		0.0039
B0174.3a	249.8(1)	11.20(5)		0.0039
B0174.4a	225.1(1)	6.50(1)		0.0039
B0117.5a	199.8(1)	1.07(3)		0.0039
B0182.1a	200.0(1)	5.04(1)		0.0039
B0182.2a	180.0(1)	1.00(1)		0.0039
N₂-broadened spectra				
B0174.1c	295.8(5)	21.90(2)	122.4(1)	0.0078
B0174.1d	295.0(5)	21.90(2)	242.5(3)	0.0078
B0174.1e	295.6(5)	5.91(1)	65.4(2)	0.0039
B0174.6b	298.0(5)	19.75(1)	798.0(1)	0.062
B0174.2b	278.0(1)	16.35(3)	184.4(2)	0.0078
B0174.2c	278.0(1)	16.35(3)	758.5(5)	0.062
B0174.2e	278.0(1)	22.35(9)	99.8(1)	0.0078
B0174.7b	278.1(1)	19.27(1)	155.2(1)	0.0039
B0174.7c	278.1(1)	19.27(1)	750.0(1)	0.062
B0174.7d	278.1(1)	19.27(1)	750.0(1)	0.062
B0174.3b	249.8(1)	11.20(5)	93.0(5)	0.0078
B0174.3c	249.8(1)	11.20(5)	262.8(2)	0.0078
B0174.4b	225.1(1)	6.50(1)	134.9(1)	0.0078
B0174.4c	225.1(1)	6.50(1)	319.4(2)	0.062
B0174.5b	199.8(1)	1.07(3)	110.5(2)	0.0078
B0181.1b	200.0(1)	5.04(1)	97.3(1)	0.0056
B0181.1c	200.0(1)	5.04(1)	299.7(1)	0.0056

Notes: P_t = total pressure; P_s = n-C₄H₁₀ partial pressure; 1 atm = 1013 mb = 760 Torr.**Fig. 1.** Vapor pressures adopted from CRC Book [34]. The vapor pressure of n-butane (in red) is seen here to be approximately one tenth of those of two other C₃H_x hydrocarbons studied in our earlier work. The butane sample pressures (in open circle) used in this study are sufficiently below the vapor pressure curve that no condensation could have occurred. [color available on-line].

tra with N₂. Measurement temperatures, 180–298 K, were chosen in consideration of a few factors, which include a broad temperature range in support of both Earth and Titan's stratosphere remote sensing, the vapor pressure of n-butane expected at the given low temperatures as shown in Fig. 1, proper sample pressures producing decent optical density, and the sample pressures producing no significant part of the absorption features being saturated.

Empty cell spectra were recorded at each given temperature, before and after taking pure and N₂-broadened spectra at the same temperature. The individual spectra, obtained across 5–6 h of scanning, were eventually coadded to spectra with the same temperature and pressures, in order to enhance the S/N. Finally, all the

n-butane spectra were ratioed to their corresponding empty cell spectra to get transmission spectra, which were used for the data analysis in this work. Neither significant drift from the true 100% transmission (*i.e.*, baseline) nor zero-level offset was noticed in the observed transmission spectrum sets. In Fig. 2, an overview of pure (in green) and N₂-broadened n-C₄H₁₀ spectra (in magenta) are presented, both of which were recorded at 278 K. A few representative band centers from *trans* and *gauche* conformers of n-butane are identified and labeled, whose complete band centers are listed in Table 3. Most of the interference features arising from residual water vapor in the FTS chamber were canceled out in the transmission spectra, though not completely. The features near 667 cm⁻¹ are CO₂ (ν₂) band from the CO₂ impurity in the n-butane sample, which survived the ratioing process by the empty cell spectrum. These CO₂ features were fitted out while generating n-butane pseudolines, which are consequently free of the CO₂ contamination. A frequency calibration factor for each spectrum was derived by comparing the observed line positions of H₂O transitions in the ν₂ band (1300–1450 cm⁻¹ region) arising from residual water in the evacuated FTS chamber with the HITRAN database 2016 [27]. The resultant frequency accuracy is estimated to be better than 0.001 cm⁻¹ for the entire set of spectra in this work.

3. Cross section measurements of n-butane (C₄H₁₀)

Butane (n-C₄H₁₀) is the simplest (all single bond) hydrocarbon exhibiting *trans-gauche* conformation. Its *trans* conformer is the more stable and abundant form due to crowding of the two methyl groups in the *gauche* structure. Their energy difference is only 0.9 kcal/mol, which makes it very hard to enrich one conformer relative to the other in the sample. However, the two conformers are spectroscopically distinctive. As listed in Table 3, with N = 14 atoms, n-butane has 36 (3N-6) fundamental vibrational modes, and their band centers are predicted by Shimanouchi (1972) [35] as reported in the NIST Chem Webbook. For the *trans* conformer, there are ten IR active bands falling into the 7–15 μm region studied in this work, and nine of them were observed. For the *gauche* conformer, there are thirteen IR active bands falling in the same region, but only eight of them were identified in our spectra. All the identified bands are presented in Table 3 along with newly suggested values of the band centers from our observed spectra. A few examples are displayed in Fig. 2, showing the absorption band features from both conformers. Note that n-butane has particularly strong bands near 1466 cm⁻¹ (~5 cm⁻¹ lower in frequency than the predicted values), which may be well covered by the Cassini/CIRS and JWST/MIRI observations. It is also important to note that this region is home to the characteristic hydrocarbon band features from CH₃ rocking, deformation, and scissoring modes. n-butane is not the only hydrocarbon that is spectroscopically active in this region. Some specific interferences with n-butane include C₂H₆ (ν₆) at 1379.2 cm⁻¹ near the n-butane ν₃₂ band, C₂H₆ (ν₈) at 1468 cm⁻¹ and (ν₁₁) at 1469 cm⁻¹ near the n-butane ν₁₄, ν₃₀, and ν₃₁ bands, and C₃H₈ (ν₅) at 1462 cm⁻¹ and (ν₁₇) at 1464 cm⁻¹ near the n-butane ν₁₄, ν₃₀, and ν₃₁ bands [30,36]. Also CH₃CN has its strongest absorption bands around 1400 cm⁻¹. If not attributed properly, the features of n-butane may be misinterpreted as contributions due to other molecules, or *vice versa*. Thus, high-resolution spectroscopy of n-butane at the selected temperatures and pressures will facilitate accurate interpretations of the CIRS spectra.

Measurements of cross-sections, σ in cm²/molecule, are straightforward. Starting with a well-defined transmission spectrum, τ_{obs}, one can derive the cross-sections by using Eq. (1)

$$\sigma = -\ln[\tau_{\text{obs}}(\nu)] / (n\xi l) \quad (1)$$

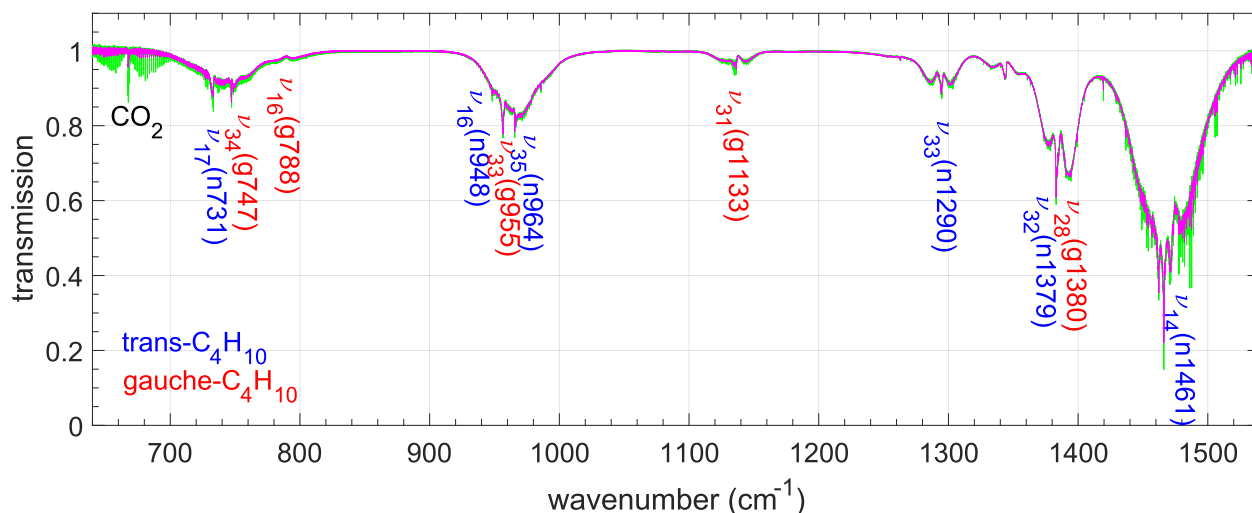


Fig. 2. An overview of pure (in green) and N_2 -mixture spectra (in magenta) of $n\text{-C}_4\text{H}_{10}$ obtained at 278 K. A few representative band centers from *trans* and *gauche* conformers are identified with a help of model predictions. For example, ν_{17} ($n731$) reads as ν_{17} band of *trans* butane conformer centered at 731 cm^{-1} . Note that the features near 667 cm^{-1} are contamination from the CO_2 (ν_2). See text for further details.

Table 3

Band centers (cm^{-1}) of the $n\text{-C}_4\text{H}_{10}$ fundamentals[#] grouped by vibrational symmetry. The bands in bold fonts in the $660\text{--}1538\text{ cm}^{-1}$ region are adopted for the vibrational partition function calculations in this work.

<i>trans</i> C_4H_{10}			
ag^s	au	bg^s	bu
ν_1 (2965,C)	ν_{12} (2968,C)	ν_{20} (2965,C)	ν_{27} (2968,C)
ν_2 (2872,C)	ν_{13} (2930,C)	ν_{21} (2912,C)	ν_{28} (2870,C)
ν_3 (2853,D)	ν_{14} (1461,C); [1466]	ν_{22} (1460,C)	ν_{29} (2853,E)
ν_4 (1460,C)	ν_{15} (1257,C); [1263]	ν_{23} (1300,C)	ν_{30} (1461,C); [1471.1, 1466.3, 1462.3 [@] ; [1466]
ν_5 (1442,D)	ν_{16} (948,B); [948]	ν_{24} (1180,D)	ν_{31} (1461,C); [1457.0] [@]
ν_6 (1382,C)	ν_{17} (731,B); [732]	ν_{25} (803,D)	ν_{32} (1379,B); [1383.3] [@]
ν_7 (1361,D)	ν_{18} (194, E) ^{&} ; [206.2 (ν_{25})] [@]	ν_{26} (225,E) ^{&}	ν_{33} (1290,B); 1294.3 [@] ; [1295]
ν_8 (1151,C)	ν_{19} (102,E) ^{&} ; [121.3 (ν_{267})] [@]		ν_{34} (1009,C) – not seen
ν_9 (1059,C)			ν_{35} (964,B); [965.8] [@]
ν_{10} (837,C)			ν_{36} (271,E); [262.0] [@]
ν_{11} (425,C)			
<i>gauche</i> C_4H_{10}			
a^s	a	b^s	b
ν_1 (2968,C)	ν_{12} (1168,D) [1175]	ν_{20} (2968,C)	ν_{27} (1450,D)
ν_2 (2968,C)	ν_{13} (1077,D); [1079] [@]	ν_{21} (2968,C)	ν_{28} (1380,C) [1384]
ν_3 (2920,D)	ν_{14} (980,D) [985.9]	ν_{22} (2920,D)	ν_{29} (1370,D)
ν_4 (2870,C)	ν_{15} (827,D) – not seen	ν_{23} (2870,C)	ν_{30} (1233,C)
ν_5 (2860,D)	ν_{16} (788,C); 798.5 [@] [790]	ν_{24} (2860,D)	ν_{31} (1133,D); [1136.5] [@]
ν_6 (1460,C)	ν_{17} (320,C)	ν_{25} (1460,C)	ν_{32} (980,D); 965.8 [@] ; [985.9]
ν_7 (1460,C)	ν_{18} (201,E) ^{&torsion}	ν_{26} (1460,C)	ν_{33} (955,C); 956.5 [@] ; [957]
ν_8 (1450,D)	ν_{19} (101,E) ^{&torsion} ; [116] [@]		ν_{34} (747,C); 747.2 [@] ; [747.4]
ν_9 (1380,C)			ν_{35} (469, D); [429.2][@]
ν_{10} (1350,C)			ν_{36} (197, E) ^{&torsion}
ν_{11} (1281,C)			

Notes: [#]The band centers in parenthesis are model predictions by Shimanouchi [35] with uncertainty codes being A(0–1 cm^{-1}), B(1–3 cm^{-1}), C(3–6 cm^{-1}), D(6–15 cm^{-1}), E(15–30 cm^{-1}). [§]Infrared inactive.

[&]Torsional bands. [@] Experimental values reported by Murphy et al. [37]. The values in square brackets are newly suggested band centers based on the observed spectra from this study.

where n , ξ , l are total number density (molecules/ cm^3), volume mixing ratio of the $n\text{-C}_4\text{H}_{10}$ in the sample, and absorption path length, i.e. 20.38 cm for all spectra in this work. As shown in the sample spectra presented in Fig. 2, the 100% transmission level was observed to be very well defined (within 0.5%), so no further adjustment or correction was needed. Cold cross-sections are measured and presented in the four separate spectral regions as listed in Table 4, which appear to be very well isolated from the neighboring bands. We report the cross-sections as measured with 99% purity sample of n -butane, but we have not attempted to discriminate the contributions from the two different conformers, which are expected to vary with the sample temperatures because of

their temperature-dependent mixing ratio at thermal equilibrium, e.g. 70% *trans* conformer and 30% *gauche* conformer at room temperature.

A sample of the measured cross-sections in the two strongest regions is presented in Fig. 3 with a comparison to that of PNNL [33]. Region I (Fig. 3a) includes the relatively well-isolated ν_{16} and ν_{35} bands at 948 (weaker) and 964 cm^{-1} (stronger), respectively, from *trans* butane, and ν_{33} at 957 cm^{-1} (stronger) and ν_{32} merged with ν_{14} at 986 cm^{-1} (weaker) from *gauche* butane. These features may be useful in identifying n -butane in the CIRS spectra, as this region ($860\text{--}1060\text{ cm}^{-1}$) of CIRS observations is not overly crowded but does contain many absorption lines from one

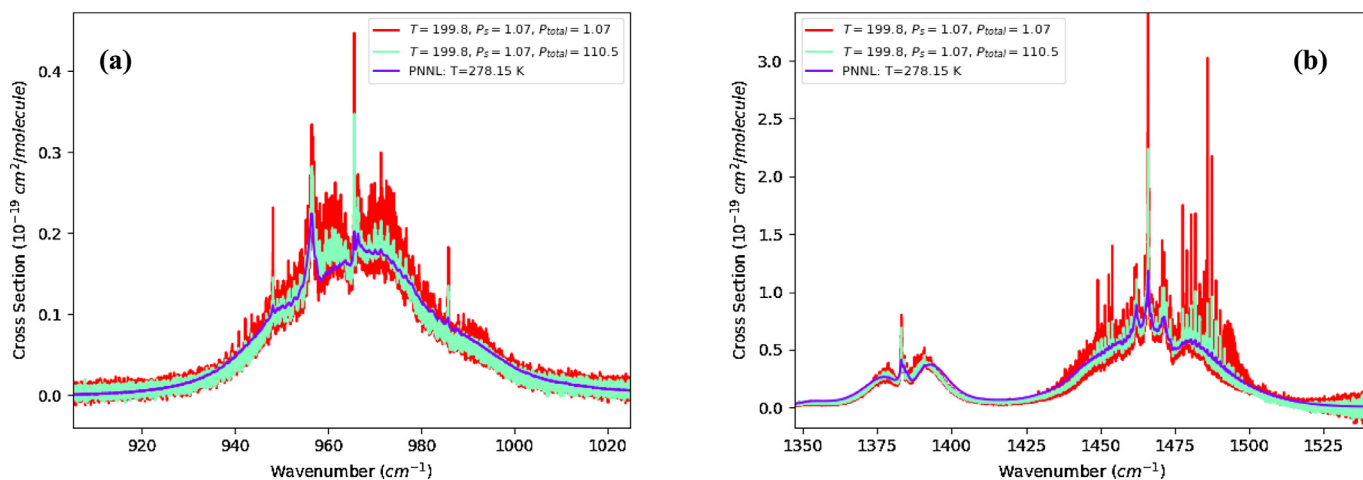


Fig. 3. Samples of cross-sections derived from the transmittances at 1.07 Torr (pure n-butane) and 110.5 Torr (N_2 -broadened n-butane); (a) for Region II: 905–1025 cm^{-1} and (b) for Region IV: 1350–1550 cm^{-1} , for the present work at 200 K (red and green curves). The measured cross-sections preserve detailed features of the n-butane absorption, which are compared with earlier work from PNNL (purple curve) obtained at much lower spectral resolution and at N_2 -loaded pressure of 1 atm. [33]. [color available on-line].

single band of C_2H_4 (ν_7) whose band center is ~ 15 cm^{-1} away from the stronger band centers, ν_{35} and ν_{33} , of the respective n-butane conformer. Fig. 3b displays Region IV, in which a multitude of fundamental bands from both conformers are overlaid ending up with two broad and strong absorption bands bearing distinctive Q-branches. One should recall that both regions presented in Fig. 3 carry substantial absorption contributions from numerous unidentified hot and combination bands, whose rovibrational transitions are smeared out to produce continuum-like absorption features. Since the cross-sections are direct measurements of the absorption features, all contributions from unidentified hot and combination bands, as well as the fundamental cold bands, are captured in the measured cross-sections. It should be also noted that detailed spectroscopic features of the measured cross-sections are not completely independent from the choice of spectral resolution. While the n-butane spectrum (presented in red) at low sample pressure (e.g. 1.07 Torr at 199 K) shows many sharp features, the spectrum of n-butane broadened by N_2 (presented in green) shows more or less smooth features in Fig. 3. Since the experimental conditions are different from spectrum to spectrum, we derived the 28 sets of cross-sections corresponding to the 28 individual spectra, which would provide sufficient data sets for extrapolation of the cross-sections at different desired temperatures and pressures within the experimental conditions as presented in Table 2.

4. Pseudoline generation

In this work, we have taken the empirical pseudoline generation approach toward developing a HITRAN [27] format pseudoline list (PLL). The pseudoline is practical parameterization to reproduce observed absorption features analogous to true spectroscopic line parameters. In brief, the mean observed coefficients over a narrow wavenumber interval may be modeled by a set of 'effective' line parameters, such as the line intensity S and lower state energy E'' , which are derived from laboratory spectra. This is accomplished by adopting a valid molecular line shape profile (e.g. Voigt profile), during which the wider the pressure and temperature ranges covered by the laboratory spectra, the more accurate and robust the pseudoline parameters can be obtained. This approach was introduced by Toon et al. [28,29] and has actually been employed in the laboratory spectrum analysis of other hydrocarbons [30–32] and in atmospheric remote sensing [28,29,38]. This

approach offers several advantages over the cross-sections measured at discrete temperature and pressure. Since the PLL was derived by fitting multiple spectra using a physical line shape model (Voigt profile) and instrumental line shape function, the resulting pseudoline parameters are independent of an instrument and spectral resolution choice. The spectral features of known impurities (such as the strong transitions from residual water and CO_2 that were observed in this work) may be modeled during the spectrum fitting, such that the PLL is ultimately generated free of those impurities. Other artifacts such as channeling and zero-level offsets (if present) can also be removed during the spectral fitting, preventing their propagation into the PLL. Moreover, the pseudoline list will be compiled in the same file format as in the public molecular spectroscopy database, e.g. HITRAN [27], such that they may be readily used in an existing line-by-line calculation model just as effectively as the true spectroscopic parameters registered in the database. Thus, while the cross-sections are specific to the pressure and temperature at which they were measured, a single pseudoline list (PLL) can reproduce the cross-sections measured at any temperature and pressure within the range of measurement temperature and pressure. Further information can be found on the JPL MK-IV website (<http://mark4sun.jpl.nasa.gov/data/spec/Pseudo/Readme>) and in the early work of our group [30–32].

We have simultaneously fitted all 28 of the n-butane spectra to generate the pseudoline parameters using a frequency grid spacing 0.005 cm^{-1} for the four different spectral regions listed in Table 4. This particular choice of frequency grid spacing offers a reasonable compromise between computation expense and retrieval precision. Effective intensities (S in $cm^{-1}/(molecule \cdot cm^{-2})$) and lower state energies (E'' in cm^{-1}) have been derived for each of the pseudoline frequencies. Additionally, we assumed N_2 - and self-broadened line widths of n-butane to be 0.12 and 0.20 cm^{-1}/atm at 296 K, respectively adapted analogously to other hydrocarbons, e.g. the ethane and benzene pressure broadening by N_2 [39,40]. For their temperature dependence exponents, a theoretical value $n = 0.72$ was adopted, where n as in $\gamma(T) = \gamma^0(296 K) \times (T/296)^n$. As stated earlier, the frequency grid spacing of 0.005 cm^{-1} was adopted to try to capture any fine spectroscopic features at low sample pressures. All the assumed parameters were supplied into the spectrum fitting process to perform line by line radiative transfer calculations per pseudoline.

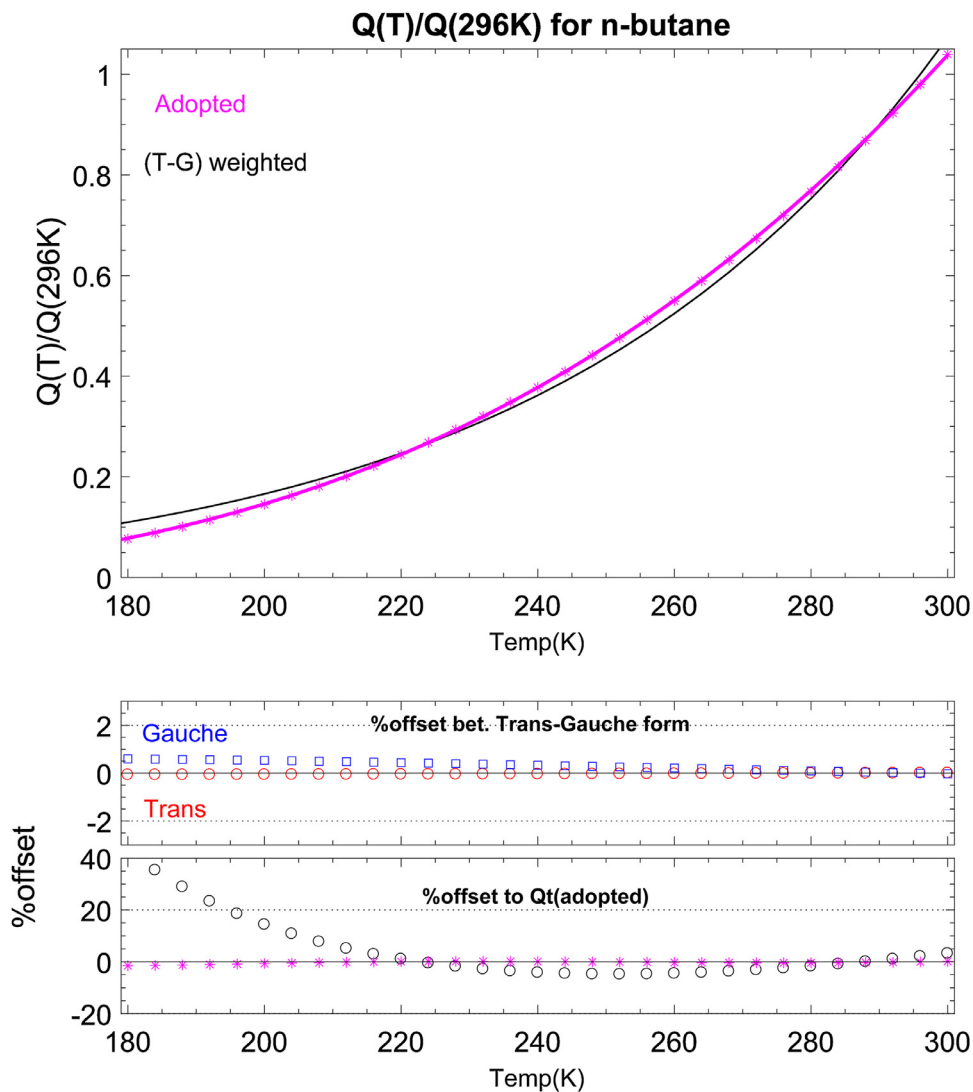


Fig. 4. (a) Trans-Gauche (T-G) weighted mean total partition function ratio (in black) is compared to the empirically adjusted total partition function (in magenta) adopted in this work. (b) The conformer-dependent deviation is estimated to be within 1% even at the extreme temperatures for n-butane. (c) However, the (T-G) weighted $Q_t(T)/Q_t(296\text{ K})$ shows an offset up to ~30% at 180 K from the adjusted total partition function ratio, $Q_t^*(T)/Q_t^*(296\text{ K})$ that has ensured the consistent multispectrum analysis.

The Voigt line shape profile is utilized to compute a high-resolution spectrum, which is subsequently convolved with the instrument line shape function (ILS) of the JPL Bruker FTS (represented by a sinc function with a field-of-view correction). The retrieved pseudoline intensities are compiled at the reference temperature $T_0=296\text{ K}$ and the lower state energies (E'') in cm^{-1} are determined via the intensity conversion expression by Eq. (2).

$$\frac{S(T)}{S_0} = \frac{Q_t(T_0)}{Q_t(T)} \frac{\exp(-c_2 E''/T)}{\exp(-c_2 E''/T_0)} \frac{1 - \exp(-c_2 \nu/T)}{1 - \exp(-c_2 \nu/T_0)} \quad (2)$$

where Q_t is the total internal partition function of n-butane, c_2 is the second Boltzmann constant (1.4388 cm/K), and ν is the pseudo-line position. The total partition function can be computed by multiplication of the vibrational partition function, Q_{vib} , and the rotational partition function, Q_{rot} , i.e. $Q_t = Q_{\text{vib}} \times Q_{\text{rot}}$. In order to fit observed spectra obtained in the wide range of temperatures, the sufficiently accurate partition function is essential to the retrieval of line intensities and the lower state energies. In this work, the total partition function was calculated in three steps. Firstly, the vibrational partition function, Q_{vib} , was computed with the Harmonic

Oscillator approximation, which can be expressed by

$$Q_v(T) = \prod_n \left\{ \frac{1}{1 - \exp(-c_2 E_{v,n}/T)} \right\}^{dgn} \quad (3)$$

where n is an index of the normal modes ($n = 1-36$ for n-butane, including the three torsional bands, ν_{18} , ν_{19} , ν_{36}). The degeneracy, dgn , is unity for all the modes, and $E_{v,n}$ is the vibrational band center of the n^{th} mode. Recalling that n-butane has two conformers (*trans* and *gauche*) with its own sets of 36 fundamental modes (i.e. vibrational band centers), the two sets of the vibrational partition functions, i.e., $Q_{\text{vib,trans}}$ and $Q_{\text{vib,gauche}}$, were computed by using their band centers listed in Table 2. It should be noted that the predicted band centers have substantial uncertainties ranging from 1–0 cm^{-1} for the low-lying states. The largest uncertainties for the band centers are those reported for torsional bands (ν_{18} , ν_{19} , ν_{36} for both *trans* and *gauche* conformers), which play a dominant role in the partition function calculations. Furthermore, we have observed that many of the predicted band centers are off from the observed band centers by a few cm^{-1} or so for the bands in the 7–15 μm region. Thus, the new values (in the brackets in Table 3) as identified from the observed spectra are

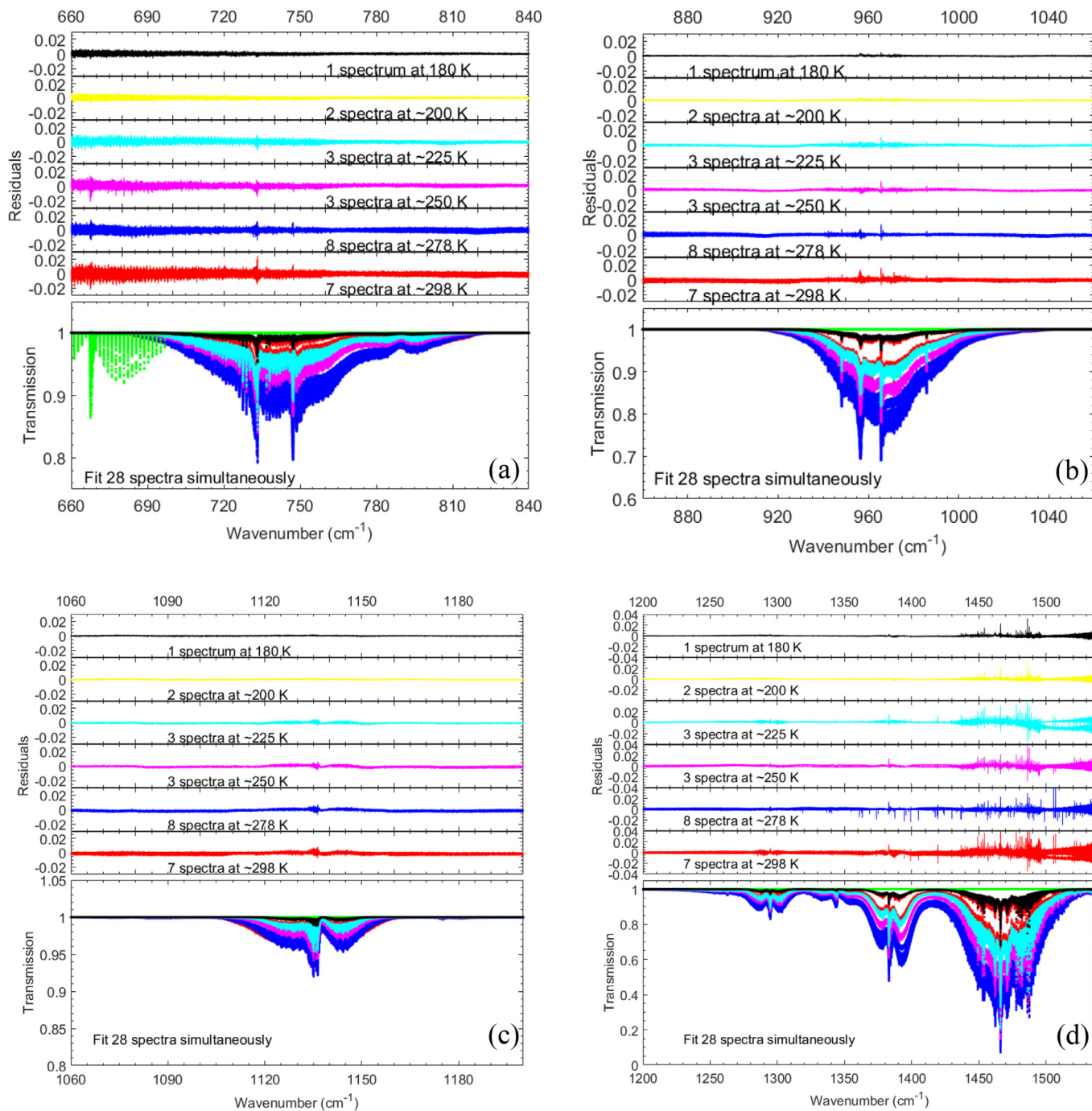


Fig. 5. Each panel (ranging ± 0.02 , i.e. 2% for Regions I, II, III and ± 0.04 for Region IV) shows the fitting residuals from all the 28 spectra. All the synthetic spectra based on the pseudolines each Region are overlaid. Note that all the CO₂ impurity features in Region I and most of the H₂O transitions in Region IV were successfully fitted out, leaving no influence to the n-butane pseudolines.

Table 4

Spectral regions defined in this work (cm⁻¹) and the observed bands in the observed spectra from this work.

Region	Coverage (cm ⁻¹)	Bands from <i>trans</i> conformer	Bands from <i>gauche</i> conformer
I	660 - 860	ν_{17}	ν_{34} , ν_{16}
II	860 - 1060	ν_{16} , ν_{35}	ν_{33} , ν_{32} , ν_{14}
III	1060 - 1200		ν_{31}
IV	1200 - 1538	ν_{33} , ν_{32} , ν_{14} , ν_{30} , ν_{31}	ν_{28}

adopted in the vibrational partition function calculations in this work. In addition to the conformer-dependent vibrational partition function, since the abundance of each conformer varies with temperature, we have adopted the weighted mean value of the two different partition functions by their mixing ratio in the sample, *i.e.* $Q_{\text{vib}} = (Q_{\text{vib,trans}} + K \times Q_{\text{vib,gauche}})/(1 + K)$, where $K = \exp(-dG_r/(RT))$, $R = 1.987 \times 10^{-3}$ kcal/mol/K, and $dG_r = 0.9 -TR \times \log(2)$ [41].

Secondly, the rotational partition function ratio at two different temperatures can be approximated by

$$Q_{\text{rot}}(T)/Q_{\text{rot}}(296\text{K}) = (T/296\text{K})^\beta \quad (4)$$

where β is the temperature dependence exponent whose values are 1.0 for diatomic molecules, 1.5 for polyatomic species with no torsional bands, but 2.0 is recommended for polyatomic species exhibiting torsional modes. Since n-butane has three torsional modes, we have adopted $\beta = 2.0$, which takes into account the substantial contributions from the torsional overtone bands and their interaction with vibrational modes, consequently enhancing total partition function. The trans-gauche (T-G) weighted total partition function is presented in the black solid line in Fig. 4(a), and their conformer-specific deviations from the T-G weighted partition function are estimated to be only a percent as shown in Fig. 4(b). It should be noted that in the actual spectrum fitting and intensity conversion as in Eq. (2), the ratio of the total partition function at a given T to that of the reference temperature, 296 K, *i.e.* $Q_r(296\text{K})/Q_r(T)$ is used.

Thirdly, the total partition function ratio, $Q_r(T)/Q_r(296\text{K})$, computed by the above two steps has been empirically adjusted to be able to reproduce all the 28 spectra obtained at the 180 – 298 K. We have observed that the retrieval of pseudoline parameters showed temperature-dependent offsets in the Volume mixing ratio Scale Factors (VSF) [which will be described in the later section], which is a strong indication of the incomplete total partition function calculations associated with the Q_r for the preliminary spectrum fitting. In fact, this finding is another benefit of doing multispectrum fitting on various spectra obtained at a broad temperature range. Any temperature-dependent inconsistency would be associated with insufficiently estimated partition function. After taking the temperature-dependent empirical correction factor into account, the adjusted total partition function, $Q_r^*(T)$, presented in magenta in Fig. 5(a), has been modeled to a third-order polynomial function for the sake of user's convenience by Eq. (5)

$$Q_r^*(T)/Q_r^*(296\text{K}) = \sum a_m T^m, \quad (5)$$

where the polynomial coefficients $a_m = (-0.02355, 0.001811, -2.595 \times 10^{-5}, 1.057 \times 10^{-7})$ with $m = 0, 1, 2,$ and 3 . As shown in Fig. 5(c), the adjusted total partition function ratio, $Q_r^*(T)/Q_r^*(296\text{K})$, can be reproduced to high precision ($\pm 0.2\%$) using Eq. (5). While the conformer-dependent deviation is confined to be within 1% even at the lowest measurement temperature as shown in Fig. 4(b), the empirical adjustment required for the consistent spectrum fitting in the temperature range (180–298 K) amounted to be more than 30% at the cold temperatures. This is not surprising because the predicted band centers, especially for low-lying states, listed in Table 1 carry huge uncertainties up to 30 cm^{-1} .

Finally, one single set of pseudolines was generated and compiled in the HITRAN format [42]. A very brief excerpt from the pseudoline list for Region 2 is presented in Table 5 to show their line parameter entries. They are molecular index (of 77, which is merely a user choice), isotopologue index (0 as for an indicator of pseudoline), line position, line intensity, and lower state energies determined from the 28 spectrum sets, and followed by other line shape parameters adopted in this work for the n-butane pseudoline generation.

Spectral fitting residuals for the N_2 -broadened n-butane spectra are presented in Fig. 5 for respective regions. Good agreement was seen to be better than 2% across the spectral regions for Regions I, II, III. The larger fitting residuals in the band center are probably because the 0.005 cm^{-1} grid spacing did not fully resolve the very fine structure of the Q-branch transitions observed in the low-pressure condition. Note that the CO_2 features near 667 cm^{-1} , as shown in green in Fig. 5a, arisen from the CO_2 sample impurity, were fitted out successfully while generating the n- C_4H_{10} pseudolines, leaving no contamination from the CO_2 features to the n-butane pseudoline list in the region. For Region 4, the fitting residuals are not as good as in the other Regions, but they are still better than 4% across the spectral region. On top of this, most of the persistent residuals are associated with water transitions rather than unaccounted n-butane absorption features. These water vapor transitions have two sources; one from the sample impurity and the other from the residual water in the evacuated FTS chamber. The former component, which survived the ratioing to get the transmission spectra, was successfully fitted out during the multispectrum fitting. However, the noise-like H_2O transition residuals are mostly due to incomplete cancelation of the residual water features arisen from the evacuated FTS chamber. However, their contribution to the absorption after having them spectrally fitted out is minimal, leaving no significant influence on the n-butane pseudoline list.

As assessment of the derived pseudoline parameters (*i.e.* intensities and lower state energies) of n-butane, we have inspected the distribution of the lower state energies vs. the line intensities, as presented in Fig. 6. The lower state energy determined at a given frequency interval (*i.e.* pseudoline position) should be regarded as an effective value representing multiple spectroscopic transitions falling in that frequency bin. Thus, the lower state energies listed in the pseudolines tend to spread out compared to the discretely distributed “true” values. Such is especially true for polyatomic hydrocarbons bearing low-lying states (*e.g.* torsional bands). In Fig. 6, the upper left portion of the pseudolines, *i.e.* strong lines with smaller values for the lower state energy, represents the transitions of a low rotational quantum number, J, from cold bands. The data points in the middle right corner represent the weak features involving higher J-transitions overlapped with those for hot band features. Lastly, the lower left part corresponds to the very weak transitions from fundamental and combination bands partially involving excited torsional bands. Collectively, the well-defined curves in Fig. 6 would represent one or two dominant bands captured in the observed spectra, *e.g.* the ν_{35} band at 966 cm^{-1} from *trans* and the ν_{33} band at 957 cm^{-1} from the *gauche* conformer of the n-butane in Region II, and ν_{31} band at 1136 cm^{-1} from *gauche* conformer in Region III. At a glance, there are multiple bands in a comparable band strength present in the Regions I and IV, which is seemingly consistent with the band centers listed in Table 2. Unlike what was seen in the pseudolines for C_3H_6 in the early work [32] in which the derived lower state energies were spread out up to $\sim 5000\text{ cm}^{-1}$, such an elongated tail of the lower state energies toward higher values is not very noticeable for n-butane pseudolines presented in Fig. 5. It is not surprising to see this unique trend since the rovibrational transitions are densely populated, arising from numerous hot and combination bands enhanced by three torsional bands of n-butane. This causes the transitions to be readily smeared out, suppressing contribution from unresolved weak lines to the derived lower state energy of the pseudoline.

For another validity test for the n-butane PLL, we performed multispectrum fitting for the 28 spectrum sets to retrieve Volume mixing ratio Scale Factors (VSF) to the experimental input n-butane sample pressure by using the PLL. Ideally, the retrieved VSFs would all be unity, confirming that the known experimental inputs listed

Table 5
An excerpt from the HITRAN-format pseudoline list for n-butane at 296 K.

MMI	freq(cm ⁻¹)	S(296 K)	N2 Self--E''	n--shift
770	965.540000	8.582E-23	0.000E+00.1200.2000	690.06600.72--0.003000
770	965.545000	8.713E-23	0.000E+00.1200.2000	588.46200.72--0.003000
770	965.550000	9.356E-23	0.000E+00.1200.2000	668.97150.72--0.003000
770	965.555000	9.024E-23	0.000E+00.1200.2000	659.60710.72--0.003000
770	965.560000	8.389E-23	0.000E+00.1200.2000	575.10120.72--0.003000
770	965.565000	8.919E-23	0.000E+00.1200.2000	715.02740.72--0.003000
770	965.570000	8.795E-23	0.000E+00.1200.2000	653.25630.72--0.003000
770	965.575000	9.191E-23	0.000E+00.1200.2000	685.03610.72--0.003000
770	965.580000	9.234E-23	0.000E+00.1200.2000	680.54050.72--0.003000
770	965.585000	8.959E-23	0.000E+00.1200.2000	594.73470.72--0.003000
770	965.590000	9.386E-23	0.000E+00.1200.2000	616.09900.72--0.003000
770	965.595000	9.239E-23	0.000E+00.1200.2000	539.73610.72--0.003000
770	965.600000	1.129E-22	0.000E+00.1200.2000	807.39280.72--0.003000
770	965.605000	9.697E-23	0.000E+00.1200.2000	467.20030.72--0.003000
770	965.610000	1.119E-22	0.000E+00.1200.2000	571.36150.72--0.003000
770	965.615000	1.072E-22	0.000E+00.1200.2000	538.32240.72--0.003000
770	965.620000	1.040E-22	0.000E+00.1200.2000	546.64760.72--0.003000
770	965.625000	1.044E-22	0.000E+00.1200.2000	534.95400.72--0.003000
770	965.630000	1.111E-22	0.000E+00.1200.2000	626.76720.72--0.003000
770	965.635000	1.154E-22	0.000E+00.1200.2000	633.26460.72--0.003000
770	965.640000	9.636E-23	0.000E+00.1200.2000	388.57240.72--0.003000
770	965.645000	1.067E-22	0.000E+00.1200.2000	554.15800.72--0.003000
770	965.650000	1.122E-22	0.000E+00.1200.2000	623.21940.72--0.003000
770	965.655000	1.077E-22	0.000E+00.1200.2000	577.92590.72--0.003000
770	965.660000	1.022E-22	0.000E+00.1200.2000	570.75240.72--0.003000
770	965.665000	1.055E-22	0.000E+00.1200.2000	632.40400.72--0.003000

Notes: MM = molecule index, 77 for n-butane; *I* = isotopologue index. Set *I* = 0 as an indicator of pseudoline entry; wavenumber in cm⁻¹; line intensity, *S*, of n-butane (99% sample) at 296 K in cm⁻¹/(molecule.cm⁻²); N₂-broadened width, Self-broadened width in cm⁻¹/atm; *E*' = lower state energy (cm⁻¹); *n* = temperature dependence exponent for pressure broadened widths; Pressure-induced frequency shifts (cm⁻¹/atm). Note that the 4th column is a placeholder for the Einstein coefficient. For further details on the data format and description, see the HITRAN database [42].

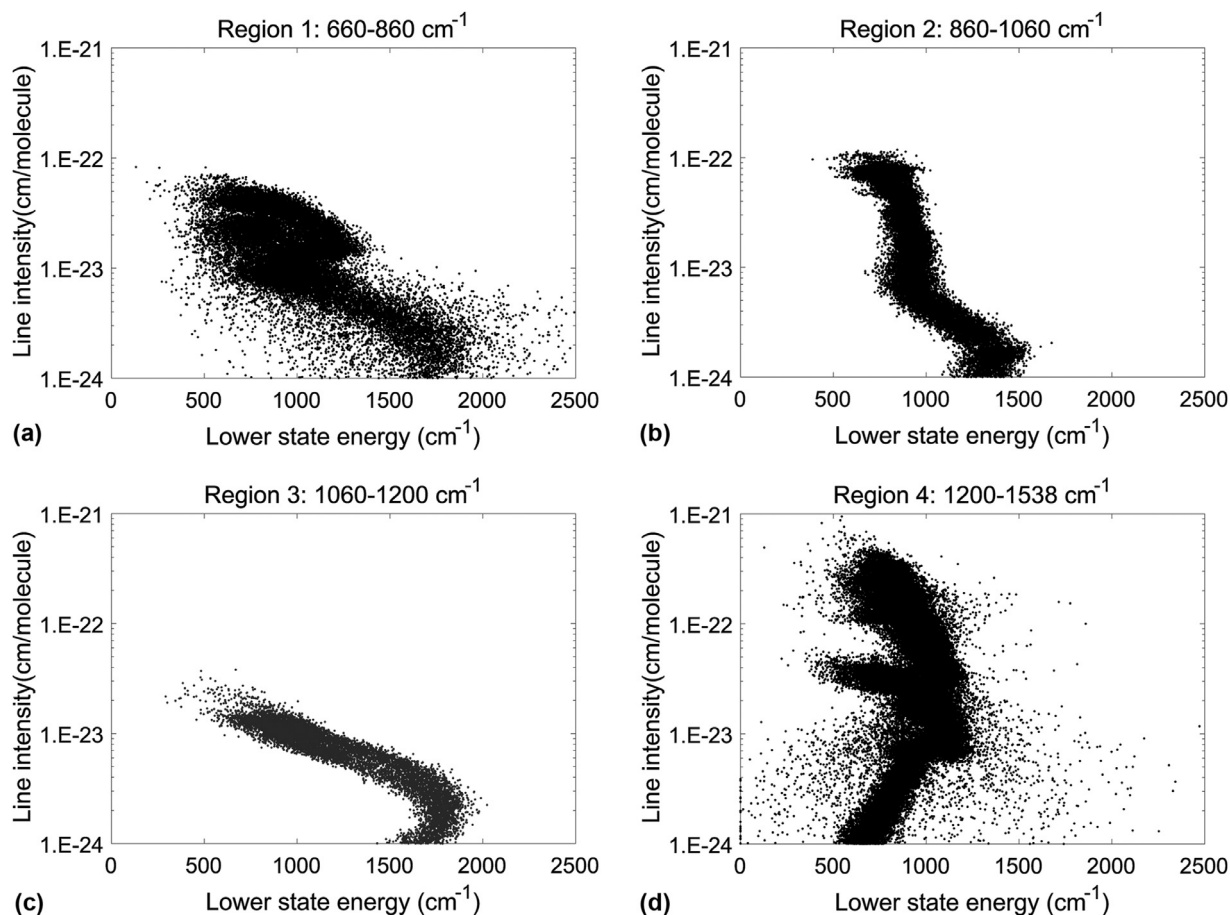


Fig. 6. Distribution of the effective lower state energies vs. the line intensities from the pseudoline list (PLL) determined by the spectroscopic region in this work.

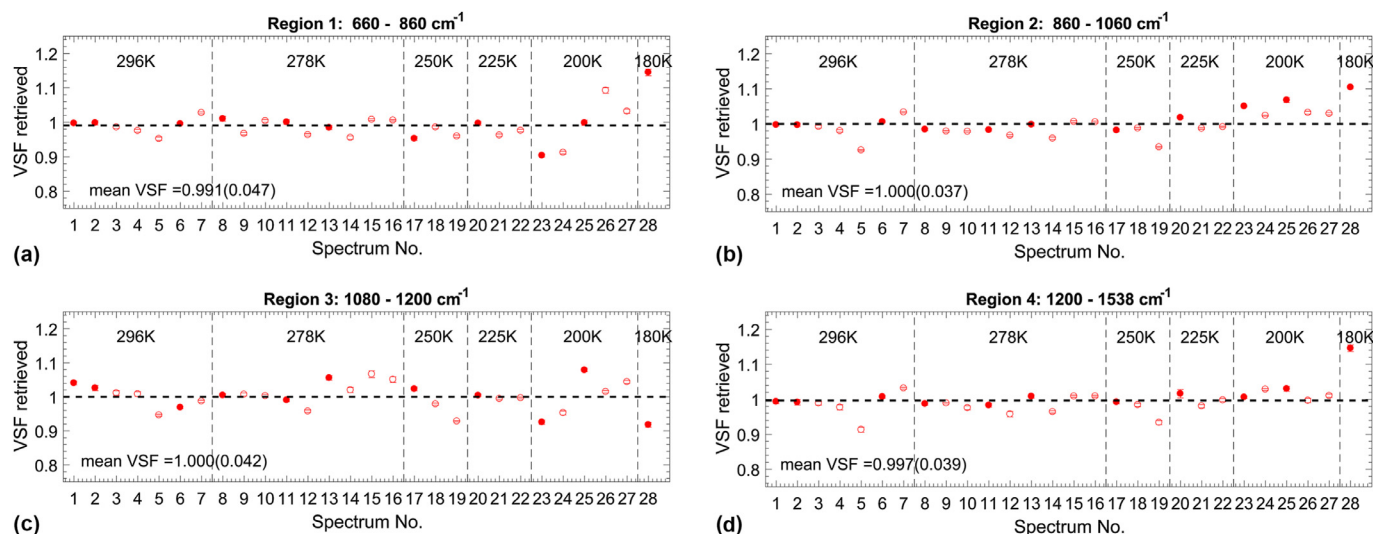


Fig. 7. Retrieved Volume mixing ratio Scale Factors (VSFs) for the respective individual laboratory spectra of the pure sample (solid circle) and of the mixtures with N_2 (open circle). The mean values of the VSFs were observed to be 0.991, 1.000, 1.000, and 0.997 for Regions I-IV, respectively, with their standard deviations less than 4.7, 3.7, 3.4, 3.9%, which can be interpreted as measurement uncertainties associated with the pseudolines.

Table 6

Integrated intensity, A_B in $10^{-19} \text{ cm}^{-1}/(\text{molecule}\cdot\text{cm}^{-2})$ of the n-butane (normalized to a 100% purity normal sample) in the region specified at various cold temperatures.

T (K)	Region I 660–860 cm^{-1}	Region II 860–1060 cm^{-1}	Region III 1060–1200 cm^{-1}	Region IV 1200–1538 cm^{-1}
298	5.06(28)	7.16(26)	0.91(4)	48.96(20)
296	5.06(28)	7.18(27)	0.91(4)	49.01(20)
278	5.08(28)	7.30(27)	0.86(4)	49.28(20)
250	5.06(28)	7.41(27)	0.77(3)	49.02(20)
225	4.99(28)	7.39(27)	0.69(3)	48.07(19)
200	4.94(28)	7.29(27)	0.60(3)	46.65(19)
180	4.97(28)	7.22(27)	0.55(3)	45.71(18)
PNNL [32]				
298	5.16	7.70	1.1	51.4
278	5.10	7.73	1.0	51.6

Notes: The measurement errors for the respective regions are based on the combined uncertainties from the mean values (bias) and their standard deviations, which are 5.6, 3.7, 4.2, and 4.0%, respectively. Overall uncertainty for the PNNL data was reported to be 3.2% [33].

in Table 2 are sufficiently accurate. Recalling that all the 28 spectra were recorded at different experimental conditions, any deviation in the spectrum-to-spectrum consistency could be interpreted as an indicator of measurement uncertainties associated with the pseudolines. Apart from the intrinsic limitations arising from the assumption made for the pseudoline generation stated earlier, there are several other factors contributing to retrieval error, which includes spectral noise, disturbance on the 100% transmission level, interfering molecules (*i.e.*, residual H_2O), and uncertainties in the experimental conditions (volume mixing ratio of n-butane, temperature, and pressure readings). As presented in Fig. 7, the mean values of the VSFs were observed to be 0.991, 1.000, 1.000, and 0.997 for Regions I - IV, respectively, showing up to 0.9% of systematic bias implicated in the pseudolines. Their corresponding standard deviations were obtained to be 4.7, 3.7, 4.2, and 3.9%, respectively, which would be interpreted as the measurement uncertainties associated with the pseudolines generated through fitting the 28 spectrum sets. Combining the systematic bias and the respective measurement uncertainties, the total measurement errors would be estimated to be no better than 6% for all four Regions.

5. Results and comparison

Since the empirical lower state energies are provided for all the individual pseudolines (*i.e.* transitions), one can obtain the pseudoline intensities at any temperatures covered our measurements (298–180 K) by using Eq. (2). The integrated intensities A_B over a given frequency range were obtained by summing the pseudoline intensities, which are compared with that of the PNNL data in Table 6 and presented in Fig. 8.

For Region I (660–860 cm^{-1}), where the ν_{17} band at 732 cm^{-1} from *trans* conformer and the ν_{34} band at 747.4 cm^{-1} from *gauche* conformer are the primary opacity sources, we note that our measurements are in an excellent agreement with the PNNL values [33] within 2% or better at both temperatures (*i.e.* 298 and 278 K). For Region II (860–1060 cm^{-1}), where the ν_{16} and ν_{35} bands from the *trans* n-butane and the ν_{33} band from the *gauche* conformer are the primary absorption bands, the integrated intensities from this work are lower than the PNNL values by 7% and 5.6% at 298 and 278 K, respectively. However, they are also in a good agreement with that of the PNNL data when considering the combined uncertainty of 6.9% (from 3.7% for PLL + 3.2% for PNNL).

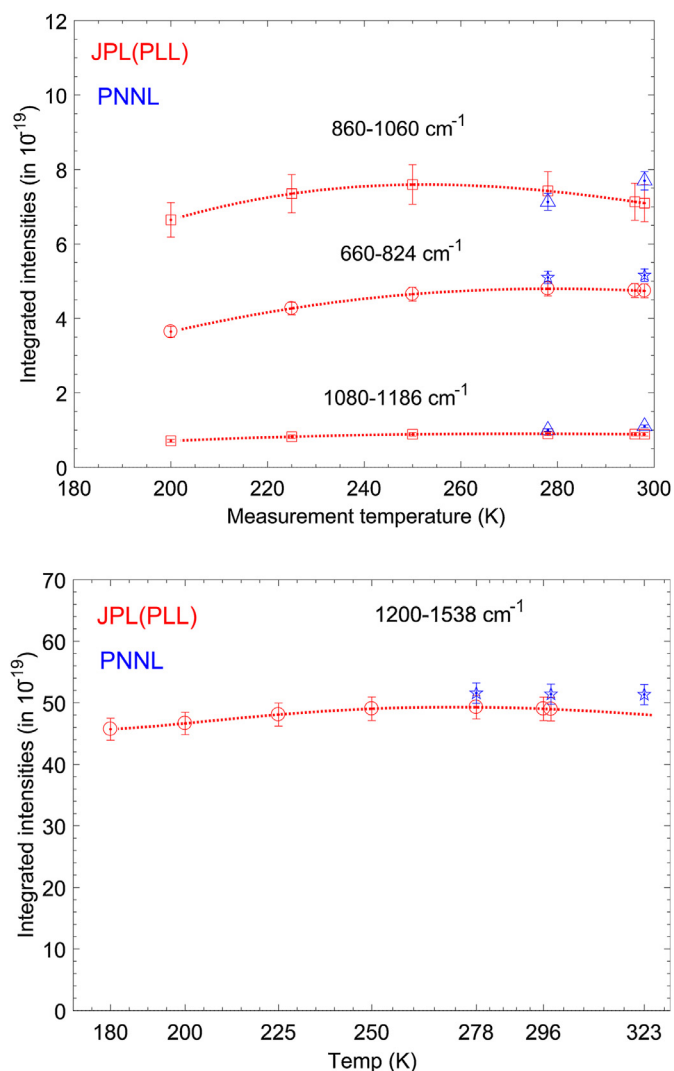


Fig. 8. Our integrated intensities ($\text{cm}^{-1}/(\text{molecule}\cdot\text{cm}^{-2})$), labeled as JPL(PLL), at various temperatures are compared to those from PNNL [33].

For Region III (1060–1200 cm^{-1}), in which the weak ν_{31} band from *gauche* conformer seems to be the only observed features, our measurements show a strong temperature dependence, dropping the integrated intensities by nearly 40% at 180 K. It implies that the substantial part of the absorption in this region is due to very weak but numerous hot band features, which become suppressed as the sample is cooled down. Our results are lower than the PNNL values [33] by nearly 17% at 298 K and by 14% at 278 K, significantly outside the combined measurement uncertainty of 7.4%. It is interesting to note that the comparable decrease in the integrated intensities is seen in the PNNL data for this Region III by 10% between 298 K and 278 K, which is greater than the decrease observed in this work, *i.e.* 5%. Also, it should be recalled that the absorption bands in this region are the weakest, so the accurate characterization of the bands may be limited in both data sets. For Region IV (1200–1538 cm^{-1}), where a few inseparable bands reside including the strongest band in the spectral region of interest for this study, the integrated intensities from this work are lower than the PNNL values by 4.7 and 4.5% at 298 and 278 K, respectively. The discrepancies are slightly greater than our measurement uncertainties, but well within the combined measurement uncertainty of 7.2% for this work and the PNNL data.

In summary, three out of the four Regions show a good agreement with the PNNL data, while Region III shows an unexplained

offset beyond the combined uncertainty. In order to characterize this region better, one would need a much longer pathlength to achieve an adequate optical density. Overall, our measurements are observed to be lower than the PNNL by a few percent, although Region I shows an excellent agreement. It is not clear what caused this discrepancy, but it should be noted that the insufficient knowledge of the partition function has hindered accurate assessment of the pseudolines. The relative abundance between *trans* and *gauche* conformers, which gradually varies from 0.70:0.30 at 296 K to 0.86:0.14 at 180 K [41], could be a significant contributor, but it is not possible to take this into account properly until all the individual transitions are distinguished by the two different conformers. We note that this discrepancy over the two conformers has not been discussed or appreciated in the PNNL data set, leaving the proper comparison with our PLL results more difficult. Finally, the rovibrational transitions of n-butane would require much higher spectral resolution at lower pressure and cold temperatures than what a conventional FT-IR can offer. Thus, an incomplete modeling of the unresolved transitions may contribute to the observed discrepancies as well.

The compiled pseudoline lists for Regions I-IV have been submitted as electronic supplements. In addition, the cold cross-sections will be submitted to the HITRAN database (<http://www.hitran.org/>) as complementary data sets. The pseudoline approach, however, may be taken as a practical interim solution to the opacity calculations for n-butane. They can be superseded by quantum-mechanically-based spectroscopic line parameters should they become available. Besides, the pseudoline list should be regarded as a mathematical construct, so that the line list would work best when they are adopted as a whole rather than as independent lines. It should also be noted that the n-butane pseudolines were strongly coupled with the specific partition function used in the multispectrum fitting and the pseudoline generation, so that one must adopt the same partition function to their line-by-line radiative transfer model calculations at temperatures covered by this work.

6. Conclusion

In support of the atmospheric infrared remote sensing of Titan from Cassini/CIRS [43] and upcoming JWST/MIRI [16], we have measured absorption cross-sections for pure and N_2 -broadened n-butane (C_4H_{10}) in the 660–1538 cm^{-1} region by analyzing 28 transmission spectra at temperatures from 180 K to 298 K. All the 28 spectra were simultaneously fitted to derive pseudoline parameters (primarily line intensities and lower state energies) on a 0.005 cm^{-1} frequency grid. For this, an effective partition function as a function of temperature was suggested by taking into account the contribution from *trans* and *gauche* conformer, as well as the empirical adjustment based on the VSFs determined from preliminary spectrum analysis. The pseudoline lists were found to be able to reproduce the observed spectral absorption to within 4% or better for all of the temperatures and pressures covered by the experimental conditions employed in this work. By summing up the pseudoline intensities, the integrated intensities were obtained, which came out to be lower than that of PNNL [33] by a few percents, but still in a good agreement within the combined uncertainties with the PNNL data.

It is worth restating that the pseudolines represent the absorption contributions from all sorts of bands (the fundamentals, excited torsional bands, hot and combination bands). The contributions from hot bands, overtone bands, and their combinations are expected to be substantial, but they are not easily tractable in quantum mechanical modeling. On the other hand, the compiled pseudolines from this work would allow accurate characterization of the observed CIRS spectra and facilitate the detection of

n-butane in the stratosphere of Titan. Likewise, the accurate characterization of the CIRS spectra with n-butane would provide a better chance of revealing new molecular features hidden in the residuals of the Cassini/CIRS spectra.

Acknowledgments

K. Sung thanks Sang Kuk Lee (Pusan Nat'l Univ., South Korea) for an informative discussion on the band centers for n-butane. The research described in this article was performed at the Jet Propulsion Laboratory, California Institute of Technology and NASA Langley Research Center under contracts with the National Aeronautics and Space Administration.

Supplementary materials

Supplementary material associated with this article can be found, in the online version, at doi:10.1016/j.jqsrt.2020.107011.

References

- [1] Clarke DW, Ferris JP. Chemical evolution on Titan: comparisons to the prebiotic Earth. *Orig Life Evol Biosph* 1997;27:225–48.
- [2] Bezdard B. Composition and chemistry of Titan's stratosphere. *Philos Trans A Math Phys Eng Sci* 2008;367:683–95.
- [3] Strobel DF. The photochemistry of hydrocarbons in the atmosphere of Titan. *Icarus* 1974;21:466–70.
- [4] Yung Y, Allen M. Photochemistry of the atmosphere of Titan: comparison between model and observations. *Astrophys J Suppl Ser* 1984;55:465–506.
- [5] Lara L, Lellouch E, Lopez-Moreno J-J, Rodrigo R. Vertical distribution of Titan's atmospheric neutral constituents. *J Geophys Res* 1996;101:23261–83.
- [6] Haye VDL, Waite J, Cravens T, Robertson I, Lebonnois S. Coupled ion and neutral rotating model of Titan's upper atmosphere. *Icarus* 2008;197:110–36.
- [7] Wilson EH, Atreya SK. Titan's carbon budget and the case of the missing ethane. *J Phys Chem A* 2009;113:11221–6.
- [8] Hébrard E, Dobrijevic M, Loison JC, Bergeat A, Hickson KM, Caralp F. Photochemistry of C₃H₄ hydrocarbons in Titan's stratospheres revisited. *Astron Astrophys* 2013;552:A132 101051/0004-6361/201220686.
- [9] Dobrijevic M, Hébrard E, Loison JC, Hickson KM. Coupling of oxygen, nitrogen, and hydrocarbon species in the photochemistry of Titan's atmosphere. *Icarus* 2014;228:324–46.
- [10] Krasnopolsky VA. Chemical composition of Titan's atmosphere and ionosphere: observations and the photochemical model. *Icarus* 2014;236:83–91.
- [11] Vuitton V, Yelle R, Klippenstein S, Hörst S, Lavvas. Simulating the density of organic species in the atmosphere of Titan with a coupled ion-neutral photochemical model. *Icarus* 2019;324:120–97.
- [12] Maguire WC, Hanel RA, Jennings DE, Kunde VG, Samuelson RE. C₃H₈ and C₃H₄ in Titan's atmosphere. *Nature* 1981;292:683–6.
- [13] Hanel R, Conrath B, Flasar FM, Kunde V, et al. Infrared observations of the Saturnian system from Voyager 2. *Science* 1982;215:544–8.
- [14] Lara LM, Lellouch E, Gonzalez M, Moreno R, Rengel M. A time-dependent photochemical model for Titan's atmosphere and the origin of H₂O. *Astron Astrophys A* 2014;143. doi:10.1051/0004-6361/201323085.
- [15] Coustenis A, Bampasidis G, Achterberg RK, et al. Evolution of the stratospheric temperature and chemical composition over one Titanian year. *Astrophys J* 2013;779:177.
- [16] Nixon CA, Achterberg RK, Ádámko vics M, Bézard B, et al. Titan science with the James Webb Space Telescope. *Publ Astron Soc Pac* 2016;128:018007.
- [17] Willacy K, Allen M, Yung Y. A new astrobiological model of the atmosphere of Titan. *Astrophys J* 2019;829:79–89. doi:10.3847/0004-637X/829/2/79.
- [18] Adamkovics M, Boering KA. Photochemical formation rates of organic aerosols through time-resolved *in situ* laboratory measurements. *J Geophys Res* 2003;108. doi:10.1029/2002JE002028.
- [19] Dobrijevic M, Loison J, Hickson K, Gronoff G. 1D-coupled photochemical model of neutrals, cations and anions in the atmosphere of Titan. *Icarus* 2016;268:313–39.
- [20] Moses JJ, Bézard B, Lellouch E, Gladstone GR, Feuchtgruber H, Allen M. Photochemistry of Saturn's atmosphere: I. Hydrocarbon chemistry and comparisons with ISO observations. *Icarus* 2000;143:244–98.
- [21] Curtis D, Glandorf DL, Toon OB, Tolbert M, McKay CP, Khare B. Laboratory studies of butane nucleation on organic haze particles: application to Titan's clouds. *J Phys Chem A* 2005;109:1382–90.
- [22] Cordier D, Cornet T, Barnes JW, Mackenzie SM, et al. Structure of Titan's evaporites. *Icarus* 2016;270:41–56.
- [23] Hewett D, Bernath P, Billinghurst B. Infrared absorption cross-sections of isobutane with hydrogen and nitrogen as broadening gases. *J Quant Spectrosc Radiat Transfer* 2019;227. doi:10.1016/j.jqsrt.2019.02.008.
- [24] Bernath PF, Bittner DM, Sibert EL. III. Isobutane Infrared bands: partial rotational assignments, ab initio calculations, and local mode analysis. *J Phys Chem A* 2019;123:6185–93.
- [25] Pickett HM. The fitting and prediction of vibration-rotation spectra with spin interactions. *J Mol Spectrosc* 1991;148:371.
- [26] Pickett HM, Poynter RL, Cohen EA, Delitsky ML, Pearson JC, Müller HSP. Submillimeter, millimeter, and microwave spectral line catalog. *J Quant Spectrosc Radiat Transfer* 1998;60:883–90.
- [27] Gordon IE, Rothman LS, Hill C, Kochanov RV, Tan T, Bernath PF, et al. The HITRAN 2016 molecular spectroscopic database. *J Quant Spectrosc Radiat Transfer* 2017;203:3–60.
- [28] Toon GC, Farmer CB, Scharper PW, Lowes LL, Norton RH. Composition measurements of the 1989 Arctic winter stratosphere by airborne infrared solar absorption spectroscopy. *J Geophys Res* 1992;97:7939–61.
- [29] Toon GC, Blavier JF, Sen B, Margitan JJ, Webster CR, May RD, Fahey D, Gao R, Del Negro L, Proffitt M, Elkins J, Romashkin PA, Hurst DF, Oltmans S, Atlas E, Schauffler S, Flocke F, Bui TP, Stimpfle RM, Bonne GP, Voss PB, Cohen RC. Comparison of Mk-IV balloon and ER-2 aircraft measurements of atmospheric trace gases. *J Geophys Res* 1999;104:26779–90.
- [30] Sung K, Toon GC, Mantz AW, Smith MAH. FT-IR measurements of cold C₃H₈ cross-sections at 7–15 μm for Titan atmosphere. *Icarus* 2013;226:1499–513.
- [31] Sung K, Toon GC, Crawford TJ. N₂- and (H₂+He)-broadened cross-sections of benzene (C₆H₆) in the 7–15 μm region for the Titan and Jovian atmospheres. *Icarus* 2016;27:438–52 Corrigendum, *Icarus* 2017; 281: 476.
- [32] Sung K, Toon GC, Drouin BJ, Mantz AW, Smith MAH. FT-IR measurements of cold propene (C₃H₆) cross-sections at temperatures between 150 and 299K. *J Quant Spectrosc Radiat Transfer* 2018:119–32.
- [33] Sharpe S, Johnson T, Sams R, Chu P, Rhoderick G, Johnson P. Gas-phase databases for quantitative infrared spectroscopy. *Appl Spectrosc* 2004;58:1452–61. <https://secure2.pnl.gov/nsd/nsd.nsf/Welcome>.
- [34] Lide DR. CRC handbook of chemistry and physics. 92th ed. New York: CRC Press; 2011.
- [35] Shimanouchi T. Tables of molecular vibrational frequencies consolidated vol. 1. national bureau of standards. nat. stand ref data ser, 39. *Nat Bur Stand (NSRDS-NBS)*; 1972.
- [36] Nixon CA, Jennings DE, Flaud J-M, Bézard B, et al. Titan's prolific propane: the Cassini CIRS perspective. *Planet Space Sci* 2009;57. doi:10.1016/j.pss.2009.06.021.
- [37] Murphy WF, Fernández-Sánchez JM, Raghavachari K. Harmonic force field and raman scattering intensity parameters of n-butane. *J Phys Chem* 1991;95:1124–39.
- [38] Irion FW, Gunson MR, Toon GC, Chang AY, Eldering A. Atmospheric trace molecule spectroscopy (ATMOS) experiment version 3 data retrievals. *Appl Opt* 2002;41:6968–79.
- [39] Devi VM, Benner DC, Rinsland CP, Smith MAH, Sams RL, Blake TA, Flaud J-M, Sung K, Brown LR, Mantz AW. Multispectrum measurements of spectral line parameters including temperature dependencies of N₂- and self-broadened half-width coefficients in the region of the ν₉ band of ¹²C₂H₆. *J Mol Spectrosc* 2010;111:2481–504.
- [40] Nadler S, Jennings DE. Foreign-gas pressure broadening parameters of propane near 748 cm⁻¹. *J Quant Spectrosc Radiat Transfer* 1989;42:399–403.
- [41] Anslyn EV, Dougherty DA. Modern physical organic chemistry. University Science Books; 2004.
- [42] Rothman LS, Jacquemart D, Barbe A, Benner DC, Birk M, Brown LR, et al. The HITRAN 2004 molecular spectroscopic database. *J Quant Spectrosc Radiat Transfer* 2005;96:139–204.
- [43] Nixon CA, Jennings DE, Bézard B, Vinatier S, Teanby NA, Sung K, Anstey TM, et al. Detection of propene in Titan's stratosphere. *Astrophys J Lett* 2013;776:L14.